

Electronic Supplementary Information (SI) for

**U-type π -conjugated phosphorescent ligand sensitized lanthanide
metal–organic frameworks for efficient white-light-emitting diode**

**Ying-Jun Chen^{a,b}, Chang-Xun Dou^b, Pei-Pei Yin^b, Jun-Ting Chen^b, Xiao-Gang
Yang^{*a,b}, Bo Li^{*a}, Lu-Fang Ma^b and Li-Ya Wang^{*a}**

*a. College of Chemistry and Pharmacy Engineering, Nanyang Normal University, Nanyang,
473061, China.*

*b. College of Chemistry and Chemical Engineering, Luoyang Normal University, Henan
Province Function-Oriented Porous Materials Key Laboratory, Luoyang 471934, P. R. China.*

*** Corresponding Author**

Tel.: 86-379-68618328, Fax: 86-20-68618320. E-mail: libony0107@nynu.edu.cn;
wly@nynu.edu.cn; yxg2233@126.com.

A. Experimental Section.

1. Materials and general procedures.

All of the materials were commercially available and used directly. All the solvents used were of analytical grade. Powder X-ray diffraction (PXRD) patterns were obtained by D/MAX-3D diffractometer. Fourier transform infrared spectra (FT-IR) were measured on BRUKER VERTEX 70v ($4000\text{-}400\text{ cm}^{-1}$). TGA patterns were collected on a NETZSCH STA 449F3 thermal analyzer with a heating rate of $10\text{ }^{\circ}\text{C min}^{-1}$ under nitrogen flow. Ultraviolet-visible (UV-vis) spectrum were recorded on UV-9000. Luminescence spectra, lifetime decays and quantum efficiency were collected on an Edinburgh FLS980 fluorescence spectrophotometer.

Optoelectronic measurements were performed with a CHI 660E electrochemical workstation (CH Instruments, Chenhua Co., Shanghai, China) by using Eu-MOF and Tb-MOF modified indium tin oxide (ITO) as the working electrode (working area 1.0 cm^2), Ag/AgCl as a reference electrode, platinum wire electrode as a counter electrode. All electrochemical tests were performed at room temperature in $0.5\text{ M Na}_2\text{SO}_4$ solution. The cyclic voltammogram curve was measured in the range of -0.6 to 0.6 V by a scan rate of 50 mV/s . The electrochemical impedance spectroscopy (EIS) measurements were recorded at the potential of -0.5 V potential in the frequency range of 0.1 Hz to 50 kHz . The system was conducted in a quartz glass reactor about 50 cm^3 , and irradiated by a 300 W Xe lamp. Transient photocurrent responses with the on-off cycle's illumination and constant potential electrolysis curves with bias

potential of -0.5 V were tested in three-electrode system at ambient pressure and room temperature.

2. Synthesis of H₄L and Ln-MOFs

Synthesis of H₄L.

A mixture of H₄L (2,6-bis(3,5-dicarboxylphenoxy)pyridine) (0.219 g, 0.5 mmol), acetonitrile (2 mL) and H₂O (2 mL) was sealed in a 25 mL Teflon-lined stainless steel vessel reactor. The mixture was heated at 120 °C for 12 hours, and then cooled to room temperature over 12 hours. Colorless block crystals of H₄L were obtained, which were washed with water several times, then dried in natural environment.

Synthesis of [Ln(HL)(H₂O)₃]_n (Ln = Eu(III), Tb(III) and Gd(III))

A similar procedure was used to obtain all complexes. For the preparation of **Eu-MOF**, a solution containing H₄L (2,6-bis(3,5-dicarboxylphenoxy)pyridine) (0.0439 g, 0.1 mmol), Eu(NO₃)₃·6H₂O (0.0446 g, 0.1 mmol), DMF (3 mL) and H₂O (2 mL) was stirred for 30 min, and then transferred to a Teflon-lined stainless steel vessel. The vessel was sealed and then heated at 140 °C for 72 h. After cooled to room temperature, the colorless crystals of **Eu-MOF** were obtained by filtration, and dried in air. Other complexes were synthesized similarly to **Eu-MOF**, except that Tb(NO₃)₃·6H₂O or Gd(NO₃)₃·6H₂O in place of Eu(NO₃)₃·6H₂O.

For **Eu-MOF**: Yield: 77.8% (based on H₄L). C₂₁H₁₆EuNO₁₃ (Mr = 642.31). Elemental analysis calcd: C 39.27, H 2.51, N 2.18%. Found: C 39.58, H 2.48, N 2.35%. IR (KBr, cm⁻¹): 1681 (m), 1611 (m), 1575 (s), 1458 (m), 1389 (s), 1300 (m), 1202 (m), 1029 (w), 944 (w), 817 (m), 673 (w), 604 (w).

For Tb-MOF: Yield: 75.5% (based on H₄L). C₂₁H₁₆TbNO₁₃ (Mr = 649.27). Elemental analysis calcd: C 38.85, H 2.48, N 2.16 %. Found: C 38.78, H 2.08, N 2.02 %. IR (KBr, cm⁻¹): 1681 (m), 1610 (m), 1577 (s), 1458 (m), 1389 (s), 1300 (m), 1204 (m), 1029 (w), 945 (w), 819 (m), 674 (w), 603 (w).

For Gd-MOF: Yield: 78.7% (based on H₄L). C₂₁H₁₆GdNO₁₃ (Mr = 647.60). Elemental analysis calcd: C 38.94, H 2.49, N 2.16 %. Found: C 39.31, H 2.44, N 3.02 %. IR (KBr, cm⁻¹): 1681 (m), 1610 (m), 1576 (s), 1459 (m), 1389 (s), 1301 (m), 1203 (m), 1029 (w), 945 (w), 818 (m), 673 (w), 604 (w).

3. X-Ray crystallography

Single-crystal X-ray diffraction measurements were performed on a Rigaku XtaLAB Pro diffractometer with Mo-K α radiation ($\lambda = 0.71073 \text{ \AA}$) at 293 K. The SADABS program was used for absorption correction.¹ All the structures were solved by direct methods and refined by the full-matrix least-squares method on F^2 with SHELXS and SHELXL programs.^{2,3} The hydrogen atoms on ligands were placed in calculated positions and refined using the riding model. The hydrogen atoms attached to water molecules were located from the difference Fourier maps and refined isotropically.

The crystalline acetonitrile molecules in H₄L are highly disordered, and attempts to locate and refine the solvent peaks were unsuccessful. A solvent mask method was used to omit the data assigned to acetonitrile molecules. Refinement parameters and crystallographic data are listed in Tables S1-S4.

4. Preparation of the LED devices

A mixture of Ln-MOF powders (50 mg) as phosphor and organic silica gel (about 2

mL) as binder was stirred for 5 min, and then carefully coated on a commercially available 365 nm purple LED. The device was heated at 100 °C for 2 h.

B. Supporting Figures

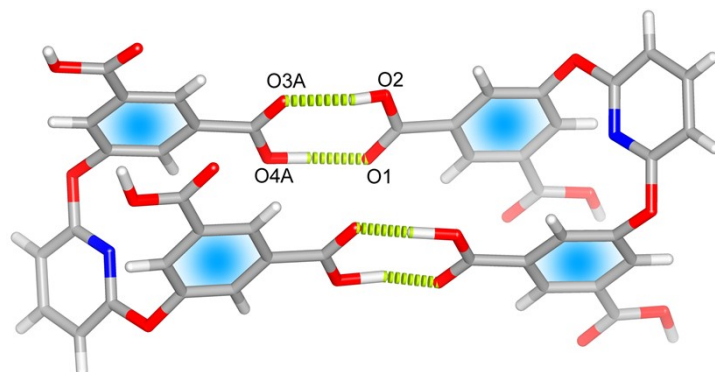


Figure S1. View of the O-H \cdots O hydrogen bonding (O2-H2 \cdots O3A and O4A-H4A \cdots O1) between the carboxyl arms in a head-to-tail mode. (Symmetry codes: A x , $1-y$, $-1/2+z$).

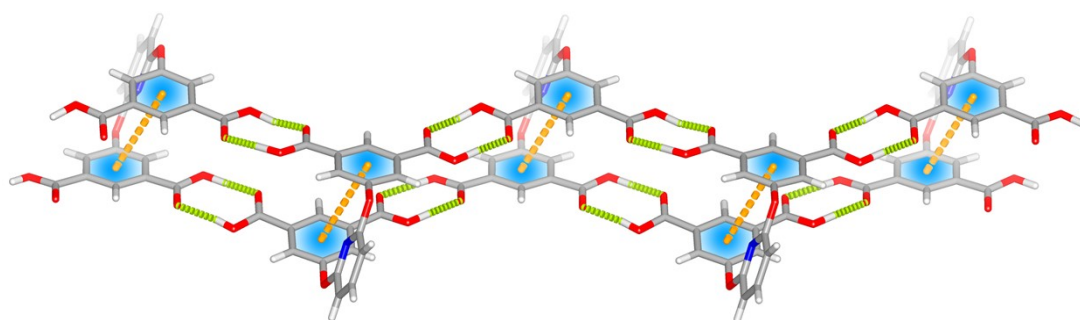


Figure S2. View of the 1D zigzag chain extended by O-H \cdots O hydrogen bonding between adjacent H₄L molecules.

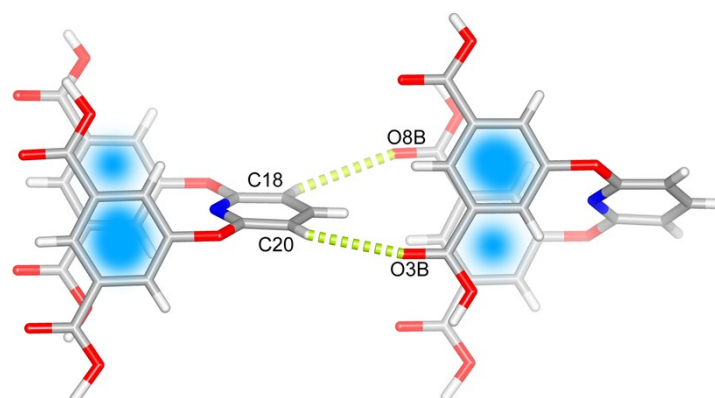


Figure S3. View of the C-H \cdots O hydrogen bonding (C18-H18 \cdots O8B and C20-H20 \cdots O3B) between the pyridine ring and carboxyl groups. (Symmetry codes: B $1/2-x$, $1/2+y$, $1+z$).

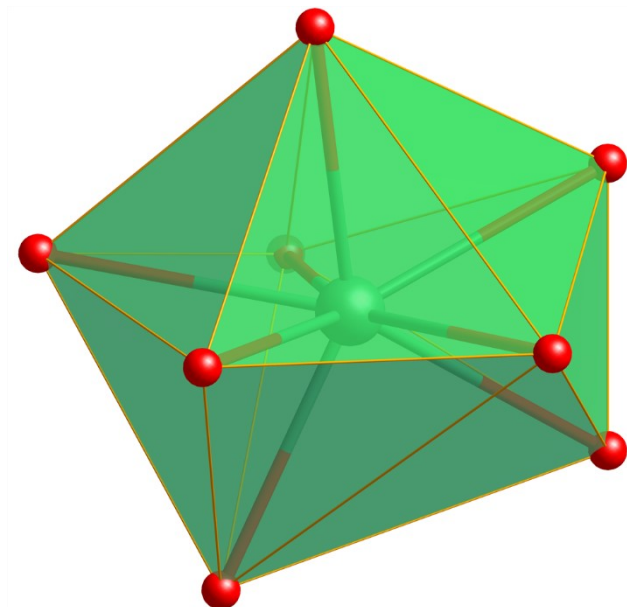


Figure S4. Coordination geometry of the Eu(III) center in **Eu-MOF**.

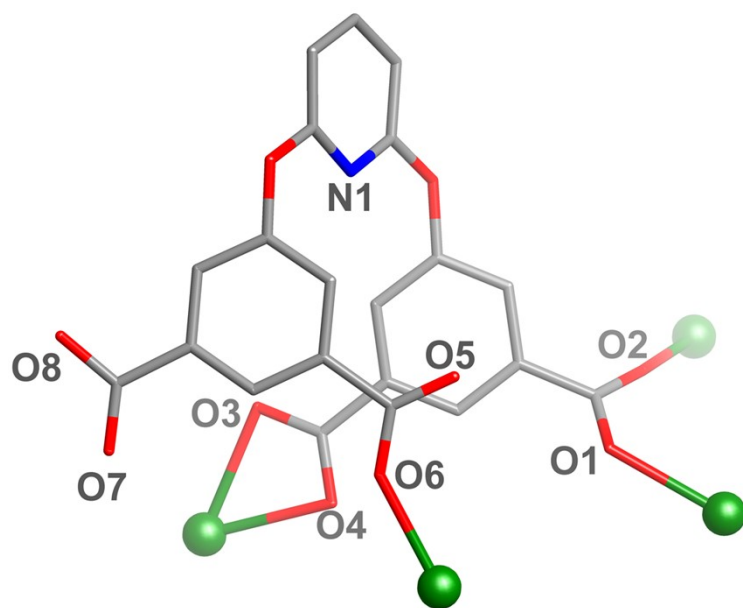


Figure S5. The coordination mode of HL ligand in **Eu-MOF**.

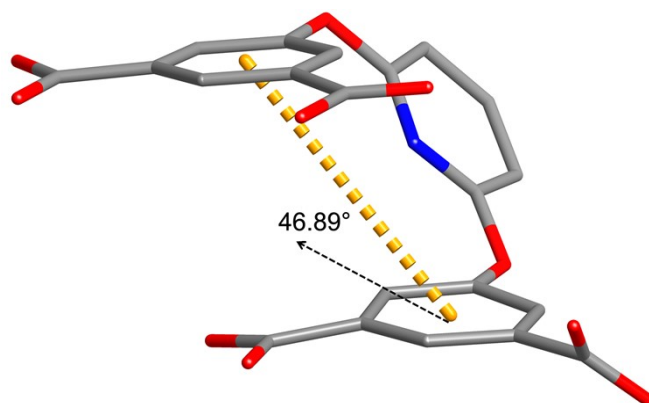


Figure S6. The configuration of HL ligand in **Eu-MOF** with a slip angle of 46.89° between benzene rings.

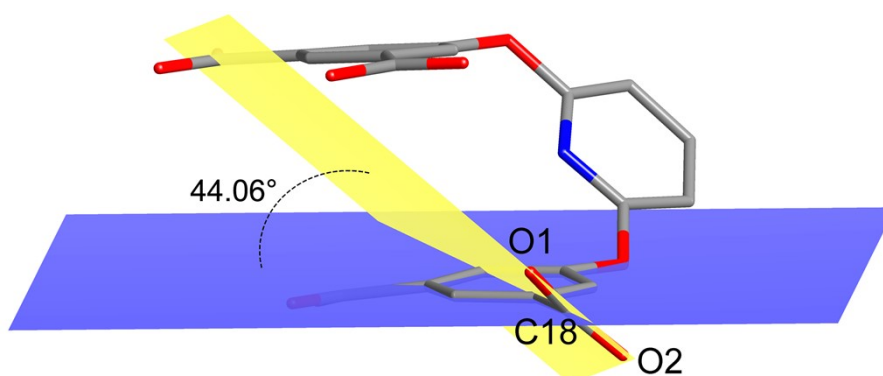


Figure S7. The torsion angle between the carboxyl group (O1-C18-O2) and benzene ring in **Eu-MOF**.

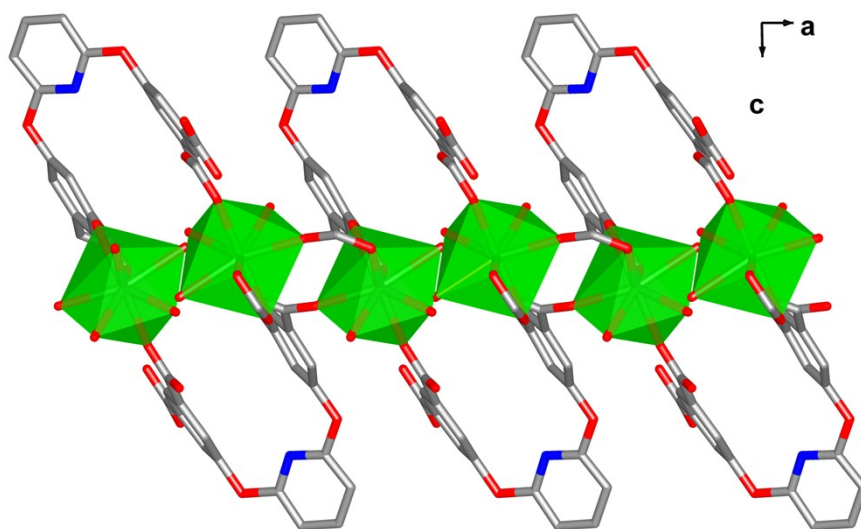


Figure S8. View of the 2D layer in **Eu-MOF** along b direction.

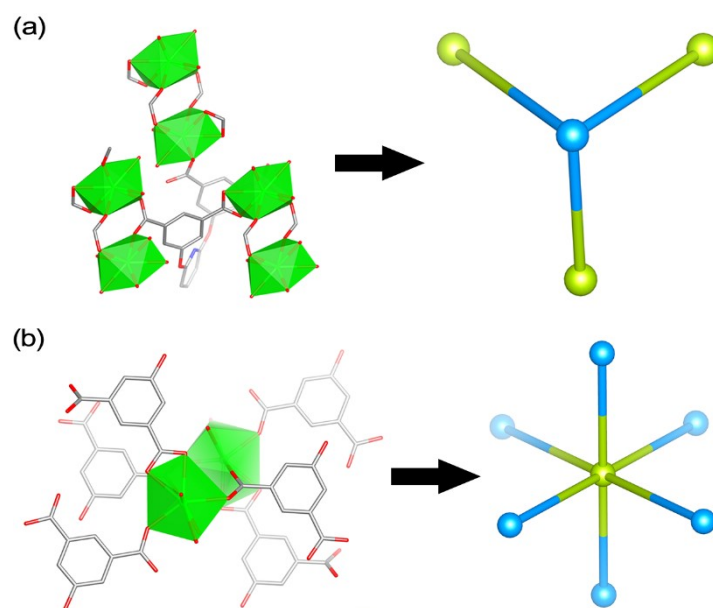


Figure S9. View of the 3-connected HL ligand (a) and 6-connected dinuclear Eu(III) unit (b) in **Eu-MOF**.

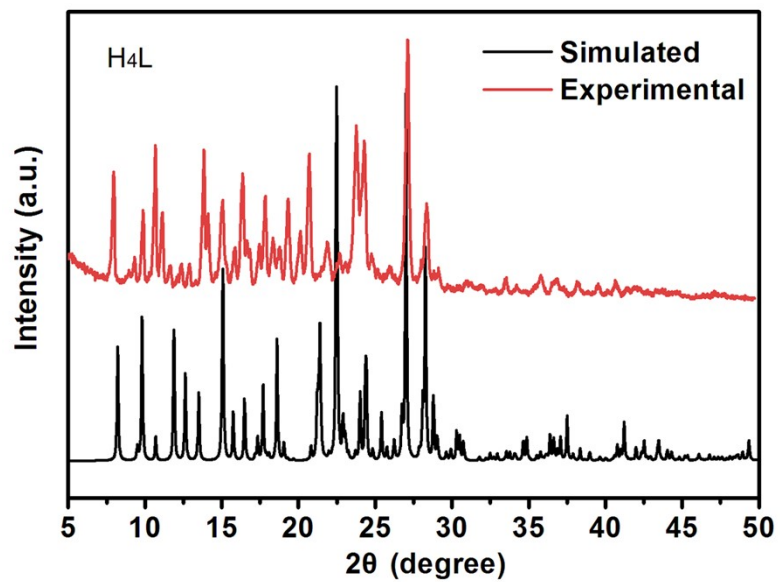


Figure S10. PXRD pattern of H₄L.

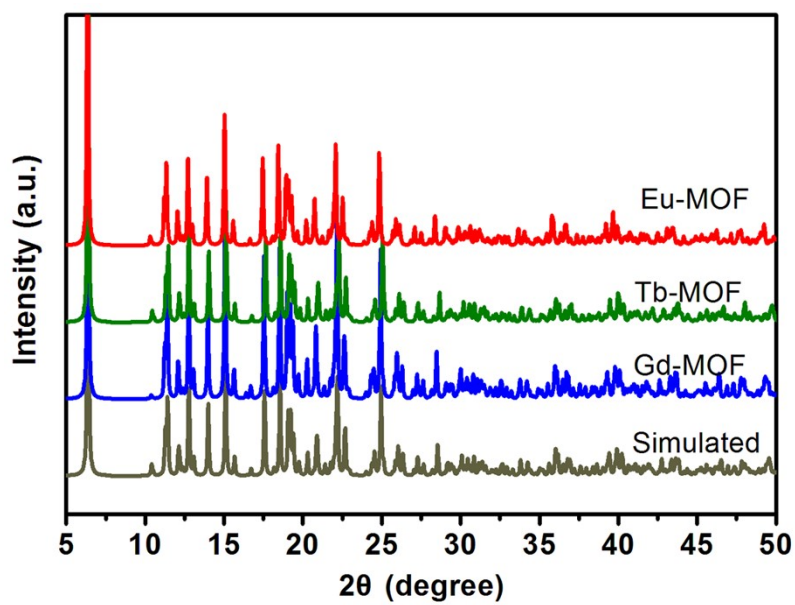


Figure S11. PXRD patterns of Ln-MOFs.

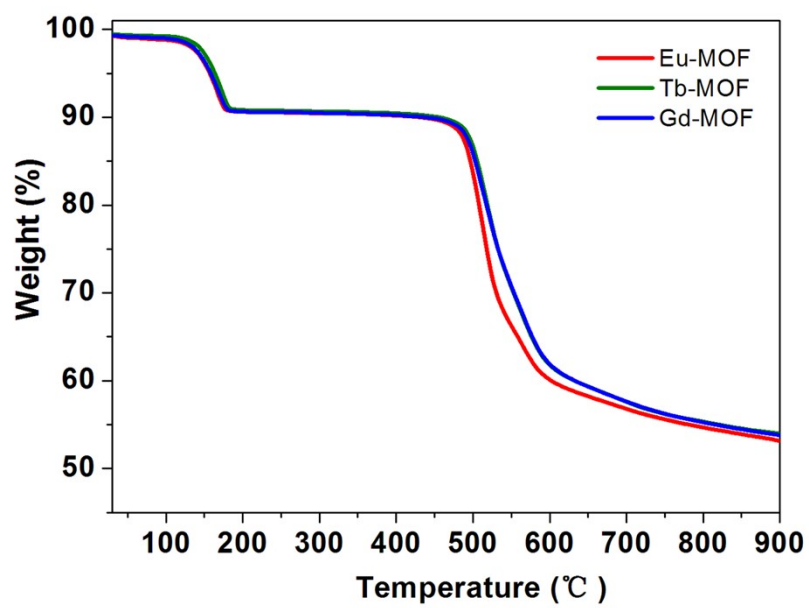


Figure S12. Thermogravimetric curves of Ln-MOFs.

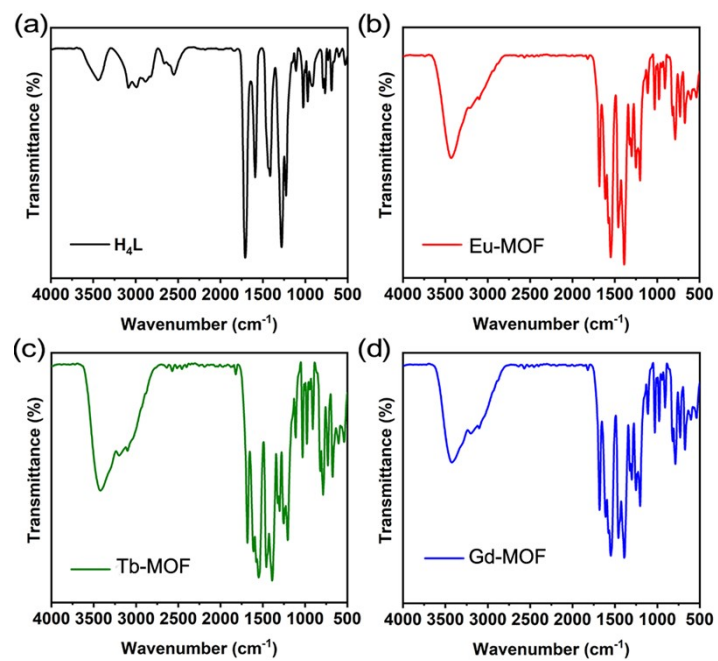
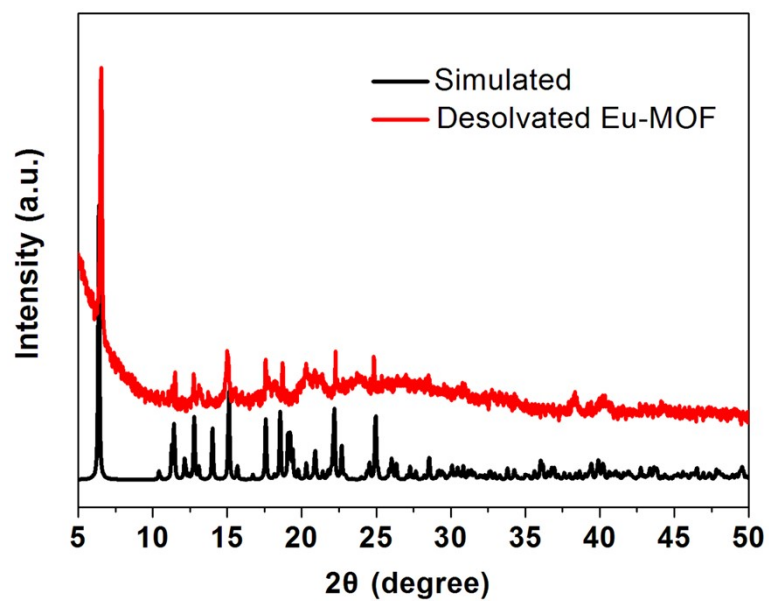
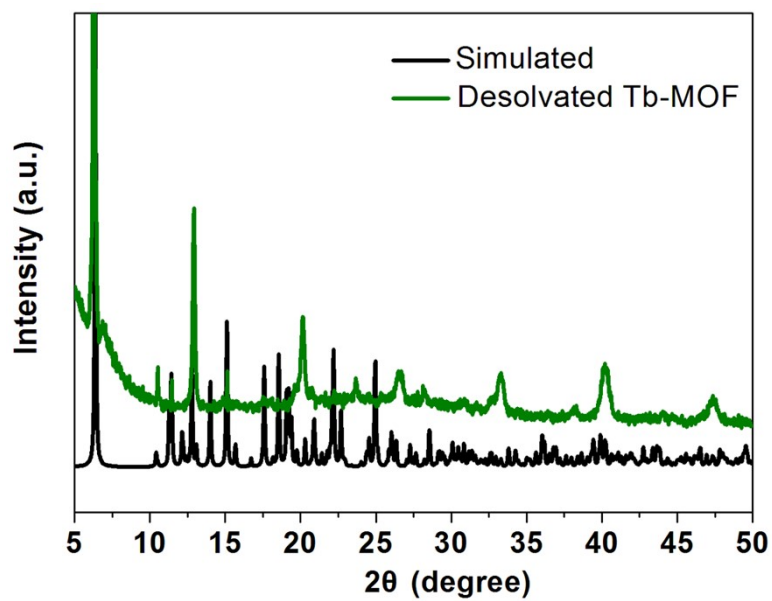


Figure S13. FT-IR spectra: (a) **H₄L**; (b) **Eu-MOF**; (c) **Tb-MOF**; (d) **Gd-MOF**.

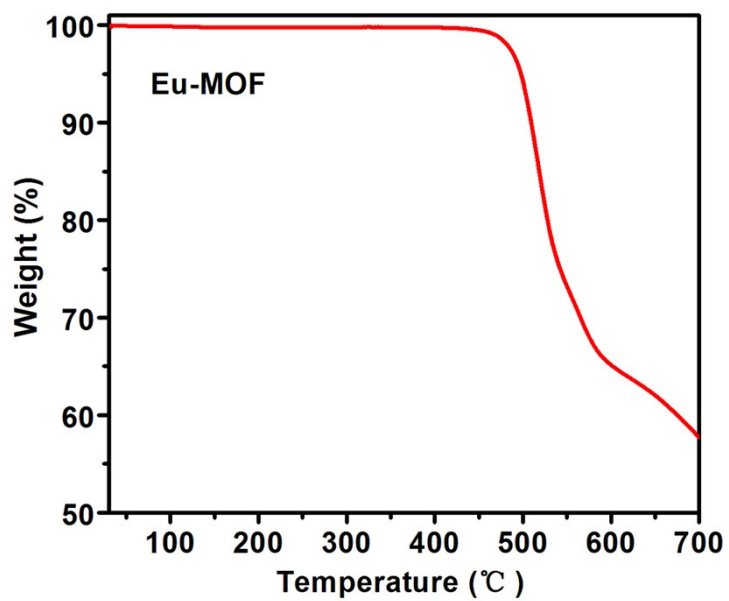


(a)

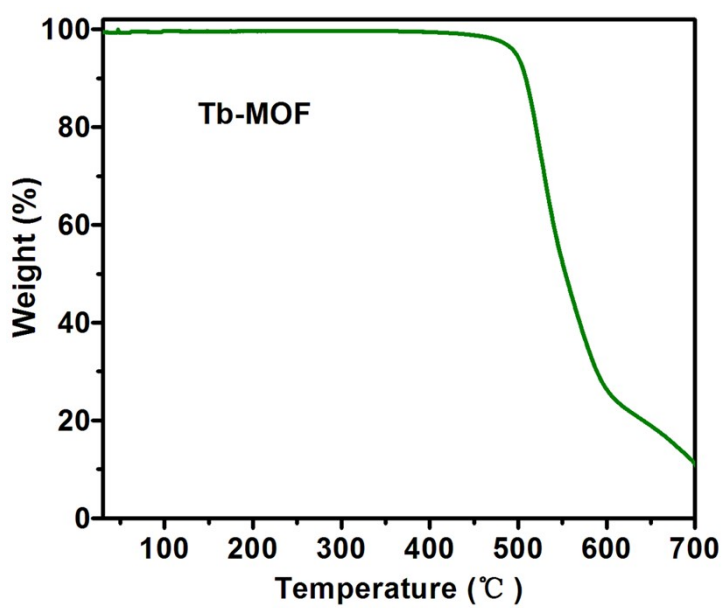


(b)

Figure S14. PXRD patterns of desolvated **Eu-MOF** (a) and **Tb-MOF** (b).



(a)



(b)

Figure S15. TGA curves of desolvated **Eu-MOF** (a) and **Tb-MOF** (b).

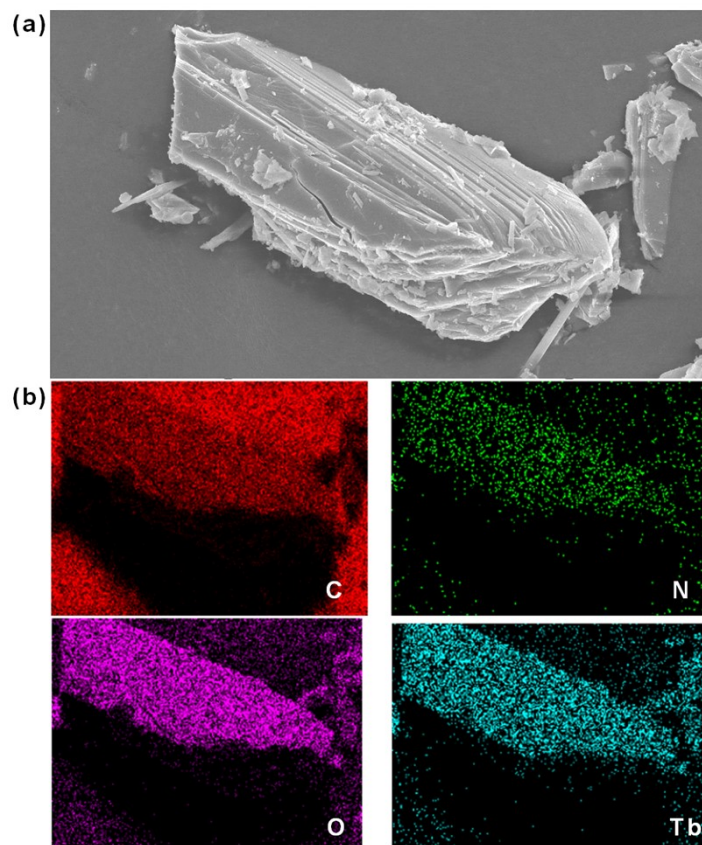


Figure S16. SEM image (a) and elemental mapping (b) of desolvated Tb-MOF.

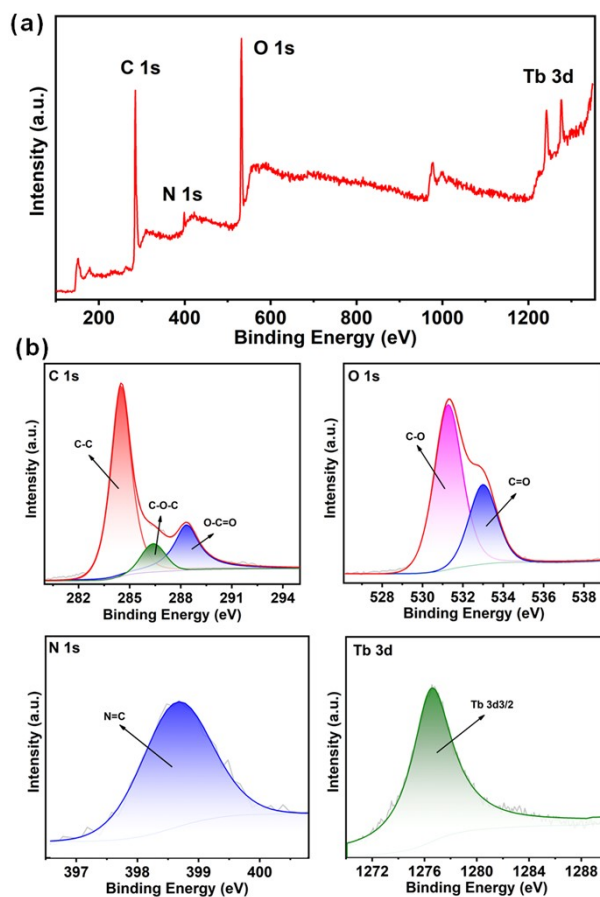


Figure S17. High-resolution XPS spectra of C 1s, N 1s, O 1s and Tb 3d_{3/2} for desolvated Tb-MOF.

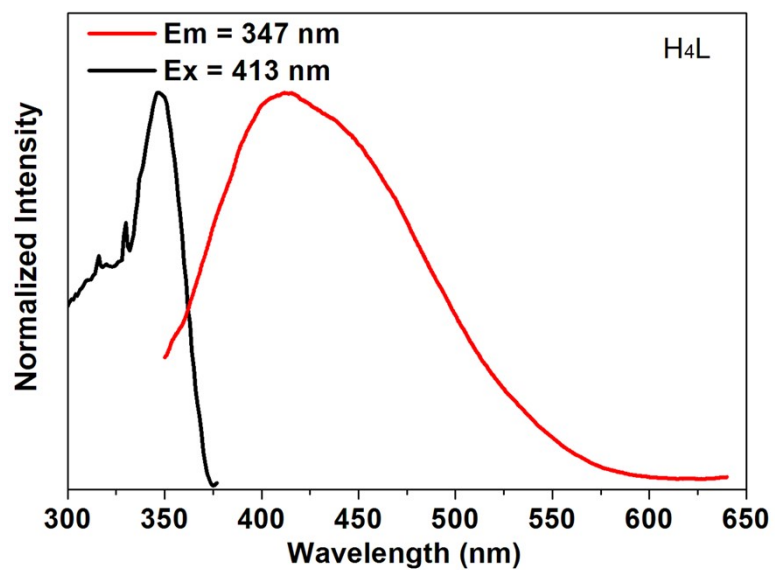


Figure S18. Normalized excitation (black line) and fluorescence emission (red line) of **H₄L** in solid state measured at room temperature.

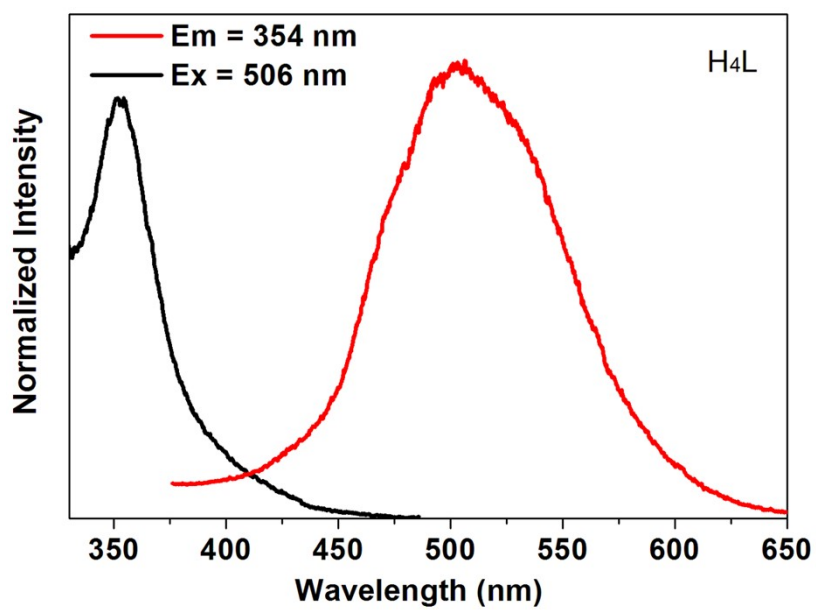


Figure S19. Normalized excitation (black line) and phosphorescence emission (red line) of H₄L in solid state measured at room temperature.

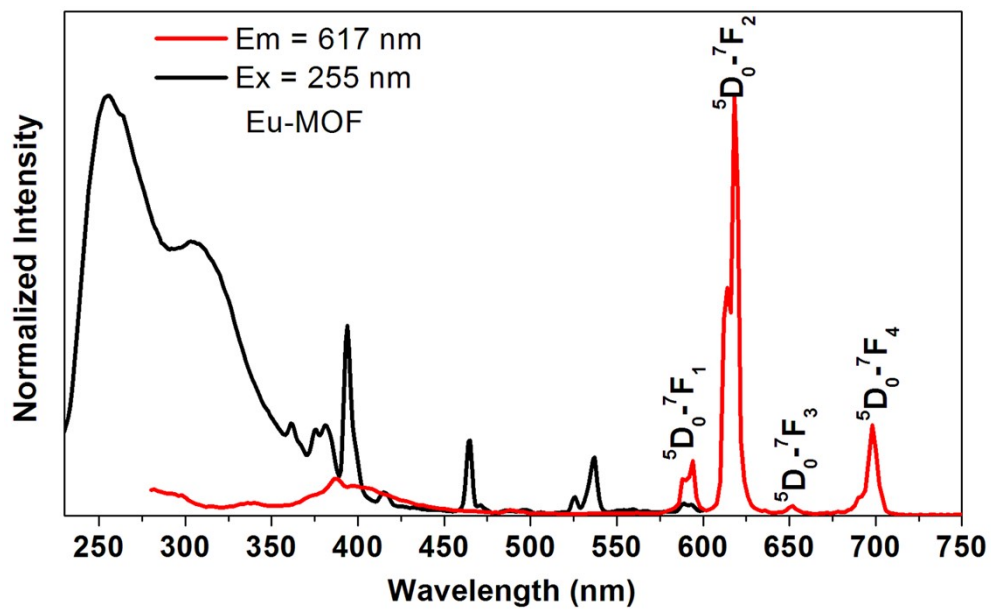


Figure S20. Normalized excitation (black line) and emission (red line) of **Eu-MOF** in solid state measured at room temperature.

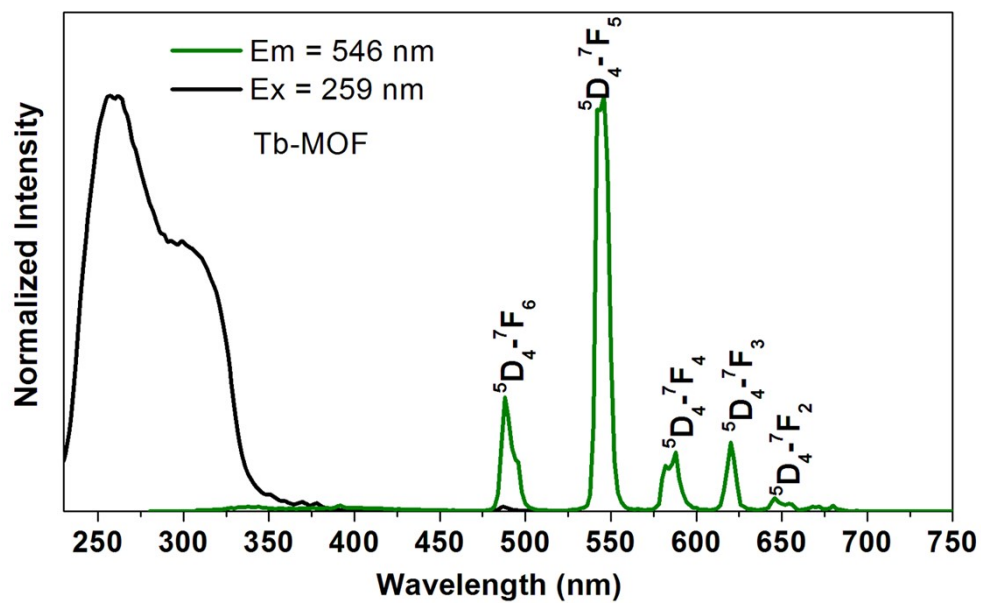
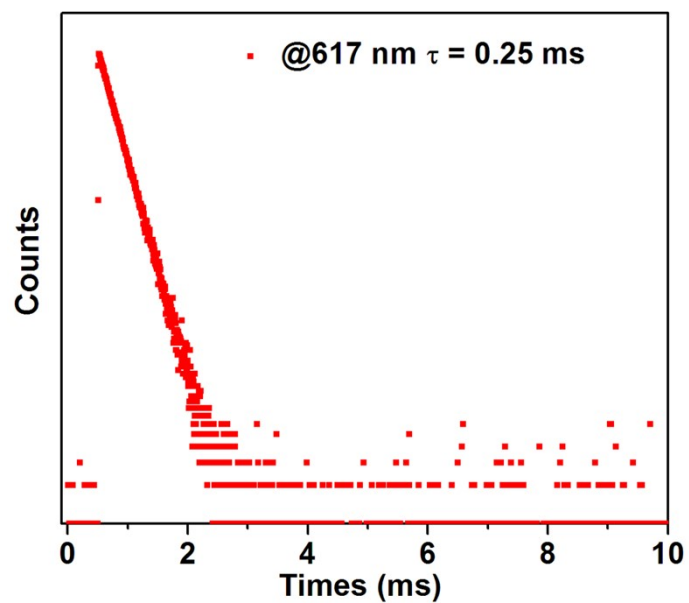
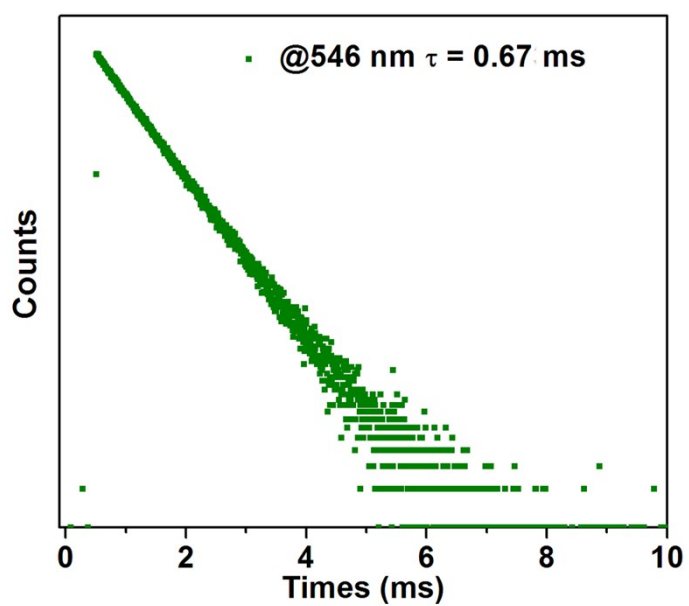


Figure S21. Normalized excitation (black line) and emission (red line) of Tb-MOF in solid state measured at room temperature.



(a)



(b)

Figure S22. Photoluminescence decay curves of Eu-MOF (a) and Tb-MOF (b) in solid state measured at room temperature.

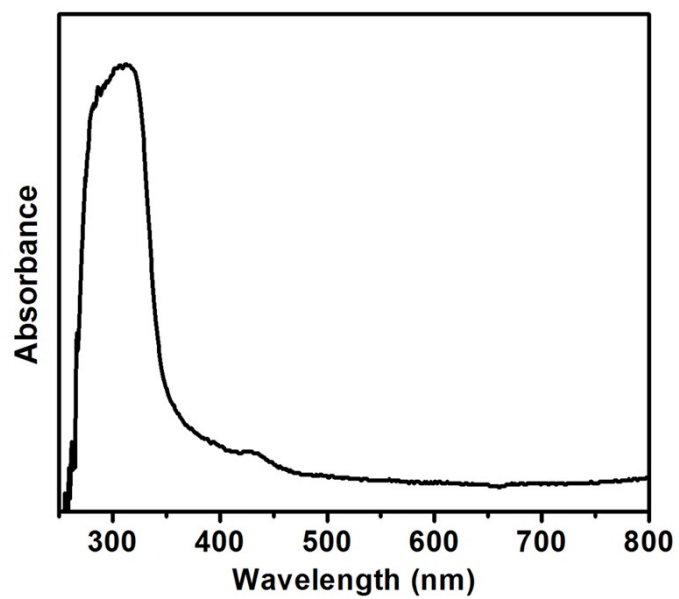


Figure S23. UV-vis absorption spectra of H₄L ligand in solid state.

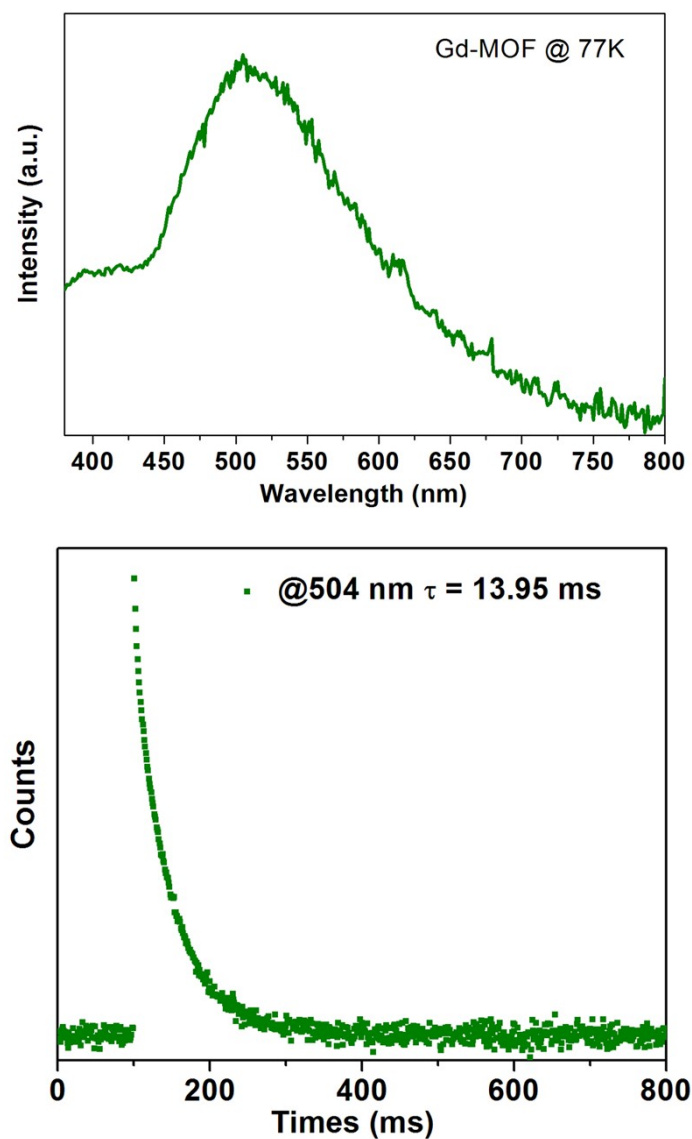


Figure S24. Phosphorescence spectrum and decay curve of **Gd-MOF** in solid state measured at 77 K.

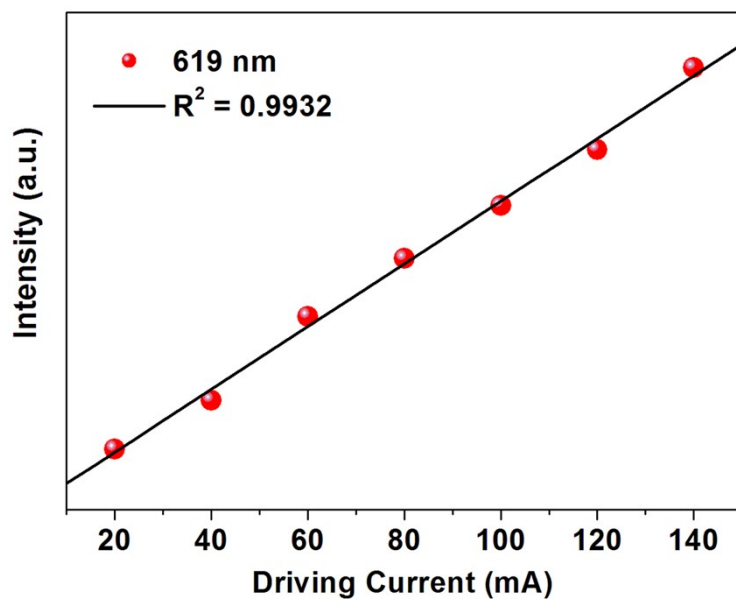


Figure S25. Relationship between the driving current and emission intensity of Eu-MOF based LED device.

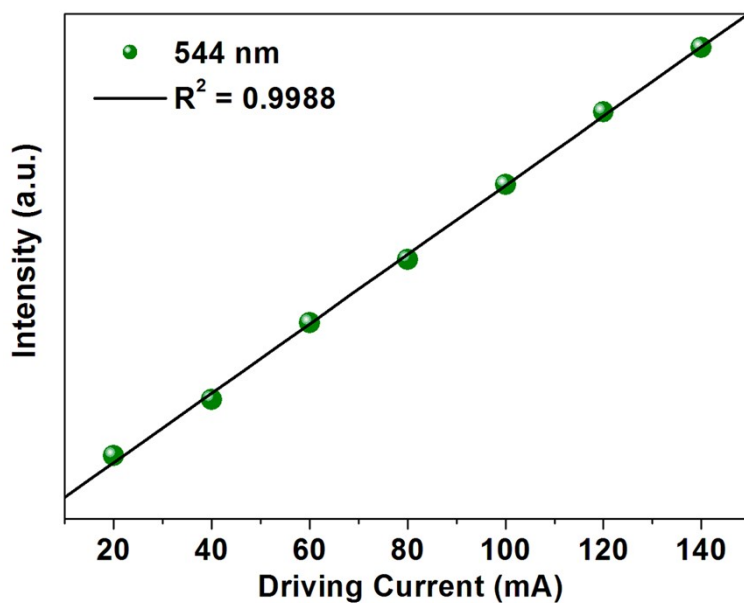


Figure S26. Relationship between the driving current and emission intensity of Tb-MOF based LED device.

C. Supporting Table

Table S1. Crystallographic data for H₄L and Ln-MOFs.

	H₄L	Eu-MOF	Tb-MOF	Gd-MOF
CCDC number	2266603	2205210	2205211	2205212
Formula	C₂₃H₁₆N₂O₁₀	C ₂₁ H ₁₆ EuNO ₁₃	C ₂₁ H ₁₆ TbNO ₁₃	C ₂₁ H ₁₆ GdNO ₁₃
Formula weight	480.39	642.31	649.27	647.60
<i>T</i> / K	293(2)	293(2)	294(2)	293(2)
Space group	<i>Pbcn</i>	<i>P</i> $\bar{1}$	<i>P</i> $\bar{1}$	<i>P</i> $\bar{1}$
Crystal system	orthorhombic	triclinic	triclinic	triclinic
<i>a</i> / Å	13.1733(10)	9.2334(5)	9.1936(5)	9.2225(5)
<i>b</i> / Å	21.389(2)	9.4545(4)	9.4195(4)	9.4553(5)
<i>c</i> / Å	16.5014(10)	14.1066(7)	14.1041(6)	14.1239(6)
α / deg	90	79.145(4)	79.170(4)	79.147(4)
β / deg	90	84.640(4)	84.543(4)	84.538(4)
γ / deg	90	65.658(4)	65.593(5)	65.581(5)
<i>V</i> / Å ³	4649.5(6)	1101.74(10)	1092.23(10)	1101.19(10)
<i>Z</i>	8	2	2	2
<i>D</i> _{calc} (g cm ⁻³)	1.373	1.936	1.974	1.953
μ / mm ⁻¹	0.110	2.921	3.313	3.086
Reflections collected	16118	9817	9846	9374
Independent Reflections	4084	5007	5045	4959
<i>R</i> (int)	0.0512	0.0322	0.0300	0.0084
<i>F</i> (000)	1985.7	632.0	636.0	634.0
GOF on <i>F</i> ²	1.055	1.044	1.038	1.031
<i>R</i> ₁ ^a [<i>I</i> > 2 σ (<i>I</i>)]	0.0818	0.0302	0.0313	0.0293
<i>wR</i> ₂ ^b (all data)	0.2473	0.0657	0.0583	0.0626

^a $R_1 = \Sigma||F_o| - |F_c||/\Sigma|F_o|$. ^b $wR_2 = [\Sigma w(F_o^2 - F_c^2)^2 / \Sigma w(F_o^2)^2]^{1/2}$.

Table S2. Selected bond lengths (Å) and angles (°) for **Eu-MOF**.

Bond	Length	Bond	Length	Bond	Length
Eu1-O1#1	2.479(2)	Eu1-O2#1	2.518(2)	Eu1-O3#2	2.383(2)
Eu1-O4#3	2.340(2)	Eu1-O5	2.297(2)	Eu1-O11	2.447(3)
Eu1-O12	2.439(2)	Eu1-O13	2.453(3)		
Bond	Angle	Bond	Angle	Bond	Angle
O1#1-Eu1-O2#1	52.31(7)	O1#1-Eu1-O3#2	132.31(9)	O2#1-Eu1-O3#2	82.56(8)
O11-Eu1-O3#2	85.42(8)	O12-Eu1-O3#2	75.66(8)	O13-Eu1-O3#2	72.20(9)
O11-Eu1-O4#3	150.03(9)	O12-Eu1-O4#3	136.92(9)	O13-Eu1-O4#3	68.66(8)
O1#1-Eu1-O4#3	80.37(8)	O2#1-Eu1-O4#3	76.33(9)	O3#2-Eu1-O4#3	105.72(8)
O5-Eu1-O1#1	77.82(8)	O5-Eu1-O2#1	129.36(8)	O5-Eu1-O3#2	147.81(9)
O11-Eu1-O5	96.59(9)	O12-Eu1-O5	74.42(8)	O13-Eu1-O5	80.52(9)

Symmetry transformations used to generate equivalent atoms: #1 1-x, 1-y, 2-z; 2# -x, 1-y, 2-z; 3# +x, -1+y, +z.

Table S3. Selected bond lengths (Å) and angles (°) for **Tb-MOF**.

Bond	Length	Bond	Length	Bond	Length
Tb1-O2	2.267(3)	Tb1-O8#1	2.303(2)	Tb1-O7#2	2.382(2)
Tb1-O12	2.410(2)	Tb1-O11	2.410(3)	Tb1-O13	2.427(2)
Tb1-O6#3	2.460(2)	Tb1-O5#3	2.492(2)		
Bond	Angle	Bond	Angle	Bond	Angle
O2-Tb1-O7#2	148.57(9)	O8#1-Tb1-O7#2	104.82(9)	O2-Tb1-O12	75.64(9)
O8#1-Tb1-O12	137.25(9)	O7#2-Tb1-O12	75.37(9)	O2-Tb1-O11	96.43(10)
O8#1-Tb1-O11	149.95(9)	O7#2-Tb1-O11	86.10(9)	O12-Tb1-O11	72.29(9)
O2-Tb1-O13	81.06(10)	O8#1-Tb1-O13	68.63(8)	O7#2-Tb1-O13	77.79(10)
O12-Tb1-O13	69.80(9)	O11-Tb1-O13	141.41(9)	O2-Tb1-O6#3	77.44(9)
O8#1-Tb1-O6#3	79.98(9)	O7#2-Tb1-O6#3	132.30(9)	O12-Tb1-O6#3	132.14(9)
O11-Tb1-O6#3	72.32(9)	O13-Tb1-O6#3	142.15(9)	O2-Tb1-O5#3	129.36(9)

Symmetry transformations used to generate equivalent atoms: #1 1+x, +y, +z; 2# 1-x, 1-y, 1-z; 3# 1-x, 2-y, 1-z.

Table S4. Selected bond lengths (Å) and angles (°) for Gd-MOF.

Bond	Length	Bond	Length	Bond	Length
Gd1-O6#1	2.288(3)	Gd1-O1	2.335(3)	Gd1-O2#2	2.387(3)
Gd1-O12	2.434(3)	Gd1-O11	2.452(3)	Gd1-O13	2.435(3)
Gd1-O3#3	2.481(3)	Gd1-O4#3	2.510(3)		
Bond	Angle	Bond	Angle	Bond	Angle
O#1-Gd1-O1	88.69(13)	O6#1-Gd1-O2#2	148.02(12)	O1-Gd1-O2#2	105.39(11)
O6#1-Gd1-O12	75.30(12)	O1-Gd1-O12	137.03(12)	O2#2-Gd1-O11	74.95(11)
O6#1-Gd1-O13	95.97(13)	O1-Gd1-O13	150.49(12)	O2#2-Gd1-O13	85.74(11)
O12-Gd1-O13	71.91(11)	O6#1-Gd1-O11	81.20(13)	O1-Gd1-O11	68.77(11)
O2#2-Gd1-O11	77.65(12)	O12-Gd1-O11	69.49(11)	O13-Gd1-O11	140.73(11)
O6#1-Gd1-O3#3	77.50(11)	O1-Gd1-O3#3	80.36(11)	O2#2-Gd1-O3#3	132.46(11)
O12-Gd1-O3#3	131.86(11)	O13-Gd1-O3#3	72.33(11)	O11-Gd1-O3#3	142.66(11)
O6#1-Gd1-O4#3	129.20(11)	O1-Gd1-O4#3	76.21(12)	O2#2-Gd1-O4#3	82.51(11)
O12-Gd1-O4#3	143.62(11)	O13-Gd1-O4#3	78.36(11)	O11-Gd1-O4#3	132.89(11)
O3#3-Gd1-O4#3	52.45(9)				

Symmetry transformations used to generate equivalent atoms: #1 -1+x, +y, +z; 2# -x, -y, 1-z; 3# -x, 1-y, 1-z.

D. Supporting References

- 1 CrysAlisPro, Rigaku Oxford Diffraction, Version 1.171.39.6a.
- 2 G. M. Sheldrick, A short history of SHELX. *Acta Crystallogr. Sect. A.*, 2008, **A64**, 112–122.
- 3 G. M. Sheldrick, SHELXT–Integrated space-group and crystal-structure determination. *Acta Cryst.*, 2015, **A71**, 3–8.